Modeling Gas Adsorption in Flexible Metal–Organic Frameworks via Hybrid Monte Carlo / Molecular Dynamics Schemes

Sven M. J. Rogge[§], Ruben Goeminne[§], Ruben Demuynck,

Juan José Gutiérrez-Sevillano, Steven Vandenbrande, Louis Vanduyfhuys,

Michel Waroquier, Toon Verstraelen, and Veronique Van Speybroeck*

Center for Molecular Modeling (CMM), Ghent University,

Technologiepark 46, 9052 Zwijnaarde, Belgium

E-mail: Veronique.VanSpeybroeck@UGent.be

Keywords: metal–organic frameworks, flexibility, gas adsorption, hybrid Monte Carlo / molecular dynamics models, breathing, phase transitions, osmotic ensemble

[§]S.M.J.R. and R.G.: These authors contributed equally

Abstract

Herein, we develop and validate a hybrid Monte Carlo (MC) / molecular dynamics (MD) simulation protocol that properly accounts for the extraordinary structural flexibility of metal-organic frameworks (MOFs). This is vital to accurately predict gas adsorption isotherms and guest-induced flexibility of these materials. First, the performance of three recent models to predict adsorption isotherms and flexibility in MOFs is critically investigated. While these methods succeed in providing qualitative insight in the gas adsorption process in MOFs, their accuracy remains limited as the intrinsic flexibility of these materials is very hard to account for. To overcome this challenge, we introduce a hybrid MC/MD simulation protocol that is specifically designed to handle the flexibility of the adsorbent, including the shape flexibility, thereby unifying the strengths of the previous models. It is demonstrated that the application of this new protocol to the adsorption of neon, argon, xenon, methane, and carbon dioxide in MIL-53(Al), a prototypical flexible MOF, substantially decreases the inaccuracy of the obtained adsorption isotherms and predicted guest-induced flexibility. As a result, this method is ideally suited to rationalize the adsorption performance of flexible nanoporous materials at the molecular level, paving the way for the conscious design of MOFs as industrial adsorbents.

1 Introduction

Whether for the storage of natural gas[1–3] or hydrogen gas[3–5] in fuel cells, the capture of greenhouse gases,[3,6] or the capture and destruction of chemical warfare agents,[3,7] the rational design of new generation materials for adsorption applications requires adsorbents exhibiting a well-defined structural nanoporosity, a large internal surface area, and a high degree of tuneability. In this respect, few materials can compete with the widespread attention metal–organic frameworks (MOFs) have drawn in the past three decades.[8–10] Composed of inorganic metal-oxide building blocks and organic ligands connected through relatively weak coordination bonds, MOFs form scaffold-like materials that usually exhibit a permanent nanoporosity.[11–13] Based on the concept of isoreticular synthesis, this porosity can moreover be modified by the incorporation of specific chemical functionalities into the material, either during synthesis or post-synthetically, without altering the underlying topology of the framework.[14,15] As a result of this tuneable and structural porosity, MOFs have been put forward as interesting platforms for gas and liquid adsorption with unprecedented storage and separation performances.[3,16–18] However, to enable the rational design and industrialization of MOFs as adsorbents, it is imperative to understand the fundamental interplay between the adsorbates and the host material that gives rise to this attractive behavior.[19] Given the challenges in the experimental characterization of adsorption in MOFs as well as the enormous amount of synthesized and hypothetical MOFs to be explored,[20] the development of computational techniques to reliably predict the adsorption performance of these materials is crucial as a complementary tool to experimental research.[21–24] Therefore, we introduce in this article a hybrid simulation protocol to predict adsorption isotherms for flexible MOFs with a substantial increase in accuracy compared to current state-of-the-art protocols. The key of this new model relies in the fact that both the gas adsorption process as well as the flexibility of the MOF, especially its shape, are properly taken into account.

From a computational point of view, modeling adsorption in MOFs is not a trivial task.[24–28] Owing to the open structures of these materials and the relatively weak coor-

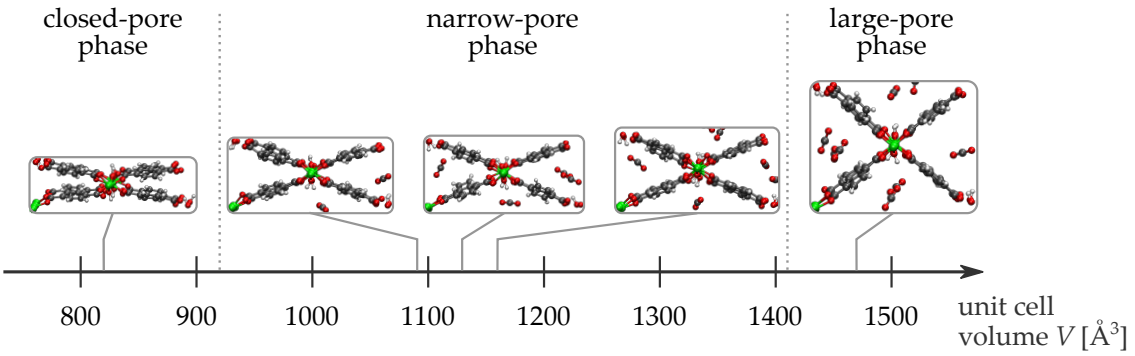

Figure 1: The closed-pore (cp), narrow-pore (np), and large-pore (lp) phases of MIL-53(Al) as encountered during CO_2 adsorption.

dination bonds between their organic and the inorganic building blocks, most MOFs exhibit a degree of structural flexibility exceeding that of conventional materials. In particular, the subclass of so-called flexible MOFs or soft porous crystals (SPCs) exhibits large-amplitude structural changes upon external stimuli such as pressure, guest adsorption, temperature, or light absorption.[22,29,30] While these structural changes may be local, *e.g.*, the gate opening observed in ZIF-8,[31] many flexible MOFs undergo large collective deformations upon external stimuli, such as the swelling in MIL-88[32,33] and the breathing in the MIL-53 family.[34] For instance, the typical winerack topology in MIL-53(Al), composed of parallel aluminum hydroxide $[Al(OH)]_\infty$ chains connected through 1,4–benzenedicarboxylate (BDC) ligands, endows this material with the topological freedom to undergo phase transitions between a large-pore (lp) and a closed-pore (cp) phase under the influence of temperature and pressure changes.[35,36] Furthermore, a narrow-pore (np) phase with an intermediate volume can be reached upon gas adsorption (see Figure 1).[34] To correctly model this flexibility and the corresponding activated phase transitions in MOFs, the development of sampling protocols specifically targeting the MOF's flexibility is a prerequisite.[37,38]

In this respect, some of us recently introduced a thermodynamic simulation protocol to model the mechanical stability of this challenging class of materials at operando conditions of temperature and pressure.[37,39] This simulation protocol relies on the observation that the unit cell volume V plays a vital role in distinguishing between the different phases in

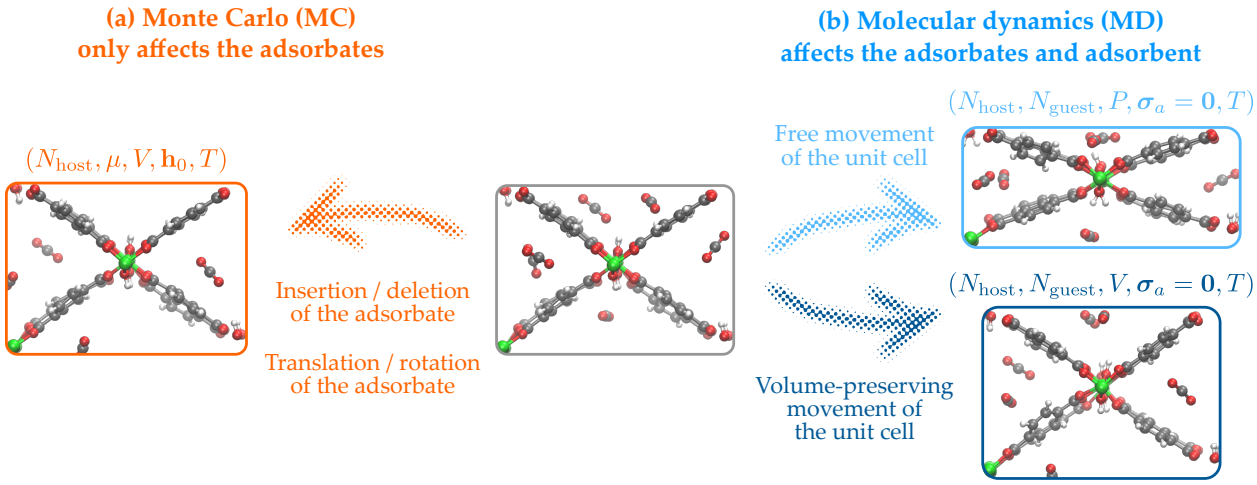

Figure 2: **(a)** Monte Carlo (orange) and **(b)** molecular dynamics (blue) simulation steps adopted to sample guest adsorption in flexible materials. For the MD steps, a distinction is made between steps that preserve the unit cell volume (dark blue) and those that affect the unit cell volume (light blue).

the majority of flexible MOFs and that their extraordinary flexibility limits the applicability of regular isothermal-isobaric molecular dynamics (MD) simulations, carried out in the $(N_{\text{host}}, N_{\text{guest}}, P, \boldsymbol{\sigma}_a = \mathbf{0}, T)$ ensemble.[37,39] Therefore, we proposed an alternative sampling technique in which the so-called pressure-versus-volume equations of state of these materials are constructed in the dedicated $(N_{\text{host}}, N_{\text{guest}}, V, \boldsymbol{\sigma}_a = \mathbf{0}, T)$ ensemble. In this last ensemble, the unit cell volume V rather than the pressure P is controlled next to the deviatoric stress $\boldsymbol{\sigma}_a = \mathbf{0}$, while still ensuring that the framework flexibility associated with the cell shape $\mathbf{h}_0$ is fully taken into account (see Figure 2(b)).[37,40] These pressure-versus-volume equations of state were observed to provide valuable microscopic insight into the mechanical stability of a variety of flexible MOFs, including MIL-53(Al),[19,37,38,40] DUT-49(Cu),[40,41] and DMOF-1(Zn).[19]

In a similar vein, several sampling techniques to model adsorption isotherms and adsorption-induced phase transitions in these flexible materials have been introduced,[19,42–47] which all rely on a sequence of Monte Carlo (MC) and/or MD simulation steps, as indicated in Figure 2. On the one hand, grand canonical MC (GCMC) trial moves are attractive as they allow not only to translate and rotate the adsorbates, but also to model adsorption by exchang-

ing guest species between the adsorbent and an external reservoir, as indicated in Figure 2(a).[24,47] However, as the adsorbent is assumed to remain rigid during this GCMC step, GCMC simulations are limited by the flexibility exhibited by the studied material.[48] On the other hand, MD moves such as those depicted in Figure 2(b) integrate the equations of motion for the guest-loaded framework as a whole, directly sampling the flexibility of the material. While these MD moves have attracted recent interest to extensively sample the flexibility in MOFs,[19,37,38] the number of adsorbed particles remains unchanged during this MD step such that adsorption isotherms cannot be directly extracted from these simulations.

Therefore, one usually adopts a well-chosen simulation protocol that combines these different MC and MD simulation steps to investigate gas adsorption in flexible materials. In literature, three distinct simulation protocols prevail, which are schematically depicted as Schemes 1 to 3 in Figure 3(a–c). A first scheme is based on conventional GCMC simulations, which were traditionally employed to model gas adsorption in rigid porous materials but neglect the potential flexibility of the material.[24,47] This shortcoming is partially addressed in Scheme 2, a hybrid MC/MD procedure in which the GCMC simulations are sequentially followed by short MD runs.[42–44] This allows the framework to deform under guest adsorption, and was succesfully adopted to predict the structural transformations of MIL-53(Cr) under CO_2 adsorption.[49] However, the method may be expected to fail when encountering high free energy barriers between the different metastable states of the host material, such as for the flexible MIL-53(Al). Finally, a third scheme was recently introduced by some of the present authors, and consists of MD simulations in the $(N_{\text{host}}, N_{\text{guest}}, V, \boldsymbol{\sigma}_a = \mathbf{0}, T)$ ensemble, fixing the unit cell volume but allowing the cell shape to fluctuate.[19,37] The pressure-versus-volume equations of state obtained within this scheme can be integrated to obtain free energy profiles, which enables one to examine the evolution of the various (meta)stable states as a function of the varying guest loading. However, this method has until now not been adopted in a hybrid MC/MD simulation protocol and it is therefore unclear whether it may be used to further increase the accuracy of the obtained adsorption isotherms.

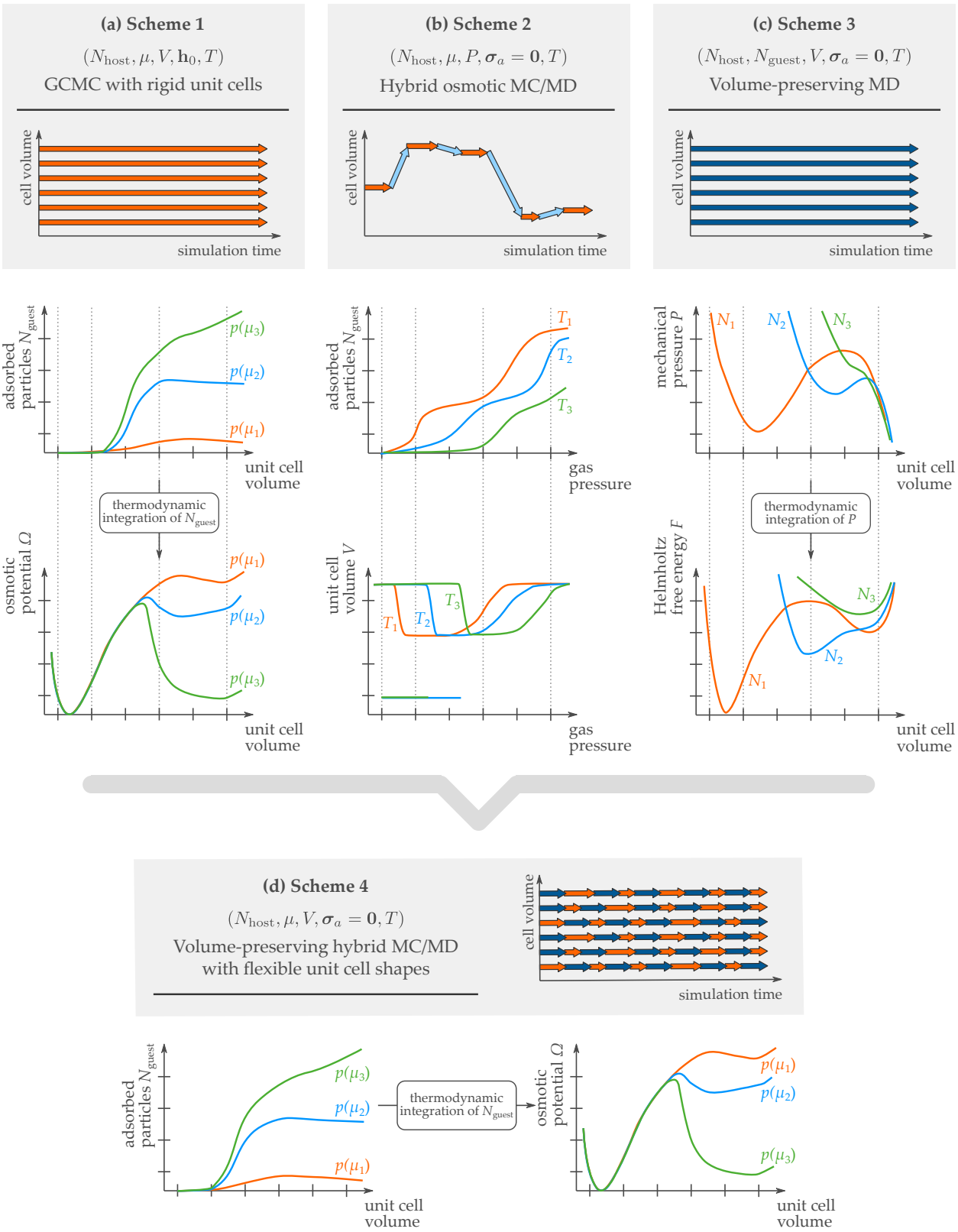

Figure 3: Schematic overview of the different combinations of MD and MC building blocks of Figure 2 that lead to the four simulation schemes discussed in this work and the thermodynamic information that can be extracted from them.

In this article, we therefore introduce a new hybrid MC/MD simulation protocol combining MC steps with MD trajectories in the $(N_{\text{host}}, N_{\text{guest}}, V, \boldsymbol{\sigma}_a = \mathbf{0}, T)$ ensemble (Scheme 4 in Figure 3(d)), which is specifically designed to handle flexible adsorbents. The performance of this newly developed hybrid MC/MD scheme to predict gas adsorption isotherms in flexible adsorbents such as MOFs and associated adsorption-induced phase transitions is critically assessed and compared to current state-of-the-art simulation protocols embedded in Schemes 1–3 of Figure 3(a–c). Its applicability is illustrated by modeling the adsorption of the noble gases neon, argon, and xenon, as well as methane and carbon dioxide, in the flexible MIL-53(Al). This choice of adsorbates is motivated by the experimentally observed breathing of MIL-53(Al) under the influence of xenon,[50] methane,[51] and carbon dioxide.[51,52] A critical comparison of the four schemes highlights the superior performance of the newly introduced scheme. As a result, this newly derived scheme is ideally suited for the further computational exploration of flexible MOFs as interesting adsorbents for a variety of gas adsorption applications.

2 Hybrid Monte Carlo / Molecular Dynamics Schemes

The four simulation protocols discussed in this article are schematically outlined in Figure 3. Before comparing their performance in the prediction of adsorption isotherms and adsorption-induced flexibility of the host material, the theory underlying these methods is briefly summarized here. In this discussion, we adopt the notation introduced in Ref. 37 to uniquely define the different thermodynamic ensembles for flexible framework materials such as MOFs. In this notation, the external stress $\boldsymbol{\sigma}$ is split into an isotropic component, the pressure $P = \text{Tr}(\boldsymbol{\sigma})/3$, and an anisotropic component, the deviatoric stress $\boldsymbol{\sigma}_a = \boldsymbol{\sigma} - P\mathbf{1}$. Likewise, the full cell matrix $\mathbf{h}$, containing the three cell vectors defining the periodic boundary conditions, is factorized into the cell volume $V = \det(\mathbf{h})$ and the cell shape $\mathbf{h}_0$ such that $\mathbf{h} = V^{1/3}\mathbf{h}_0$.

Scheme 1: GCMC Simulations with a Rigid Unit Cell in the Restricted Osmotic Ensemble

The first scheme, depicted in Figure 3(a), finds its roots in conventional GCMC simulations. These simulations, carried out in the $(N_{\text{host}}, \mu, V, \mathbf{h}_0, T)$ ensemble, were traditionally employed to model gas adsorption in rigid porous media such as rigid MOFs at a given chemical potential μ and temperature T.[24,47] To also simulate flexible materials, exhibiting multiple (meta)stable states, this original protocol was embedded into Scheme 1, in which a series of these GCMC simulations are performed in parallel for a limited set of different adsorbed configurations (see Figure 3(a)).[45] For many flexible materials, such as MIL-53(Al), these configurations can be defined by the unit cell volume of the material. As indicated in Figure 3(a), Scheme 1 gives rise to adsorption isotherms in the so-called restricted osmotic ensemble.[21,45,46] As the cell shape $\mathbf{h}_0$ is kept fixed during these simulations, these isotherms will be referred to as rigid-host isotherms $N_{\text{guest}}(N_{\text{host}}, \mu, \mathbf{h}_0, T; V)$. These rigid-host isotherms can afterwards be transformed towards the osmotic potential by thermodynamic integration of the isotherms with respect to the chemical potential:

$$\Omega(N_{\text{host}}, p, \mathbf{h}_0, T; V) = F_{\text{host}}(N_{\text{host}}, T; V) + pV - \int_{-\infty}^{\mu(p,T)} N_{\text{guest}}(N_{\text{host}}, \mu', \mathbf{h}_0, T; V)\mathrm{d}\mu', \quad (2.1)$$

A similar procedure was followed in the derivation of the OFAST model by Coudert and co-workers.[21,45,46] From this osmotic potential, the (meta)stable phases of the system at a given temperature and gas pressure as well as its adsorption capacity can be extracted (see Figure 3(a)).[21]

Scheme 2: Hybrid MC/MD Simulations in the Osmotic Ensemble

In the second scheme, depicted in Figure 3(b), the osmotic or $(N_{\text{host}}, \mu, P, \boldsymbol{\sigma}_a = \mathbf{0}, T)$ ensemble is sampled.[42–44] In this thermodynamic ensemble,[53] not only the number of adsorbed

guest molecules may vary during the simulation, as in Scheme 1, but also the framework is allowed to deform under guest adsorption and external stress $\boldsymbol{\sigma} = P\mathbf{1} + \boldsymbol{\sigma}_a$. To sample the osmotic ensemble, a hybrid MC/MD procedure is considered, depicted schematically in Figure 3(b). Besides the translation, rotation, insertion, and deletion of the guest molecules considered in the GCMC steps (orange arrows in Figure 3(b)), which are again carried out in the $(N_{\text{host}}, \mu, V, \mathbf{h}_0, T)$ ensemble, also short MD simulations in which the guest-host system is propagated in time according to the $(N_{\text{host}}, N_{\text{guest}}, P = p, \boldsymbol{\sigma}_a = \mathbf{0}, T)$ ensemble (light blue arrows in Figure 3(b)) are considered as MC trial moves in this hybrid scheme.[42–44] Here, the external pressure P is controlled to equal the gas pressure p, which is related to the chemical potential μ through the van der Waals equation of state. This hybrid (osmotic) Monte Carlo (HOMC) approach was succesfully adopted before to qualitatively predict the structural transitions and adsorption isotherms of MIL-53(Cr) upon CO_2 adsorption.[49] However, the presence of unsurmountable free energy barriers between the different adsorption-induced metastable states of the host material as well as large volume fluctuations of the MOF unit cell during these simulations may limit the accuracy of this method.[37,38]

Scheme 3: Advanced MD Simulations of the Guest-Loaded Framework at Constant Volume

A third method to predict guest-induced flexibility in MOFs was recently introduced by some of the present authors.[19,37] As shown in Figure 3(c), this method relies on a series of MD simulations in the $(N_{\text{host}}, N_{\text{guest}}, V, \boldsymbol{\sigma}_a = \mathbf{0}, T)$ ensemble that only fix the cell volume while allowing the cell shape to fluctuate.[37,40] In these simulations, the cell volume V is controlled, whereas the cell shape $\mathbf{h}_0$ is allowed to fluctuate so to counteract, on average, the zero deviatoric stress $\boldsymbol{\sigma}_a = \mathbf{0}$. At equilibrium, the average internal pressure during such a simulation indicates the pressure the material can withstand at the given volume. By repeating this procedure for a range of volumes, the finite-temperature pressure-versus-volume equation of state at a given guest loading, $P(N_{\text{guest}}, T; V)$, can be extracted (see

Figure 3(c)). From these pressure profiles, the corresponding Helmholtz free energy profiles $F(N_{\text{guest}}, T; V)$—the finite-temperature analogue of the energy-versus-volume equations of state—can be derived via thermodynamic integration:[37,54]

$$F(N_{\text{guest}}, T; V) - F(N_{\text{guest}}, T; V_{\text{ref}}) = -\int_{V_{\text{ref}}}^{V} P(N_{\text{guest}}, T; V')\mathrm{d}V'. \tag{2.2}$$

By determining the (local) minima in the free energy profile, this method identifies the different (meta)stable states at a given guest loading even if they are separated by substantial free energy barriers. While this method was originally introduced to investigate pressure-induced phase transitions in empty MOFs,[37] the procedure was extended in Ref. 19 to also account for adsorption-induced transitions. In this modified procedure, the $(N_{\text{host}}, N_{\text{guest}}, V, \boldsymbol{\sigma}_a = \mathbf{0}, T)$ simulations are carried out not only for the empty framework ($N_{\text{guest}} = 0$), but also for the adsorbate-loaded framework ($N_{\text{guest}} > 0$). By tracking the different metastable states as a function of the guest loading, this method allows for the identification of adsorption-induced flexibility in MOFs. Furthermore, the osmotic potential can be obtained by considering the Legendre transform of the Helmholtz free energy profile, as outlined in more detail in Ref. 55.

Scheme 4: Hybrid MC/MD Simulations with a Flexible Unit Cell in the Restricted Osmotic Ensemble

To circumvent the disadvantages associated with the previous three schemes, a hybrid MC/MD procedure is introduced in this article. This new hybrid procedure, depicted as Scheme 4 in Figure 3(d), samples the $(N_{\text{host}}, \mu, V, \boldsymbol{\sigma}_a = \mathbf{0}, T)$ ensemble. To this end, one starts from the procedure outlined in Scheme 1, which samples the rigid-host or $(N_{\text{host}}, \mu, V, \mathbf{h}_0, T)$ ensemble. To go beyond this approach and ensure a proper sampling of the atomic positions and the cell shape, an MD trajectory is considered as an additional MC trial move in Scheme 4, akin to Scheme 2. However, while the MD trajectory in Scheme 2 is performed in the $(N_{\text{host}}, N_{\text{guest}}, P = p, \boldsymbol{\sigma}_a = \mathbf{0}, T)$ ensemble, here, the $(N_{\text{host}}, N_{\text{guest}}, V, \boldsymbol{\sigma}_a = \mathbf{0}, T)$ ensemble of

Scheme 3 is sampled, so that the volume remains conserved while fully sampling the cell shape and atomic positions. This hybrid MC/MD scheme therefore results in flexible-host isotherms, $N_{\text{guest}}(N_{\text{host}}, \mu, \boldsymbol{\sigma}_a = \mathbf{0}, T; V)$, in contrast to the rigid-host isotherms of Scheme 1. These isotherms can then be transformed to the flexible-host osmotic potential:

$$\Omega(N_{\text{host}}, p, \boldsymbol{\sigma}_a = \mathbf{0}, T; V) = F_{\text{host}}(N_{\text{host}}, T; V) + pV - \int_{-\infty}^{\mu(p,T)} N_{\text{guest}}(N_{\text{host}}, \mu', \boldsymbol{\sigma}_a = \mathbf{0}, T; V) \mathrm{d}\mu'. \tag{2.3}$$

3 Results and Discussion

3.1 Scheme 1: GCMC Simulations with a Rigid Unit Cell in the Restricted Osmotic Ensemble

3.1.1 Noble Gas Adsorption

Given the experimentally observed breathing of MIL-53(Al) under the influence of xenon adsorption at room temperature,[50] the 300 K rigid-host isotherms of Scheme 1 were first constructed for neon, argon, and xenon. The resulting adsorption isotherms are visualized in Figure 4(a,b) and Figure S1 of the Supporting Information. At the lowest MIL-53(Al) cell volumes, no uptake is observed for any of the three guest species. Adsorption only starts to take place once the cell volume is increased above 950 Å^3, 1025 Å^3, and 1100 Å^3 for neon, argon, and xenon, respectively. At these volumes, the diameter of the MIL-53 channels starts to exceed the kinetic diameters of these guest species, as indicated in Figure S3, allowing for the adsorbates to be accommodated in the channels.

However, even for sufficiently large unit cell volumes, the uptake of neon and argon in MIL-53(Al) remains small, amounting to only 0.4 atoms (neon) or 1.5 atoms (argon) per unit cell. This low uptake can be explained by the low adsorption energies for both gases

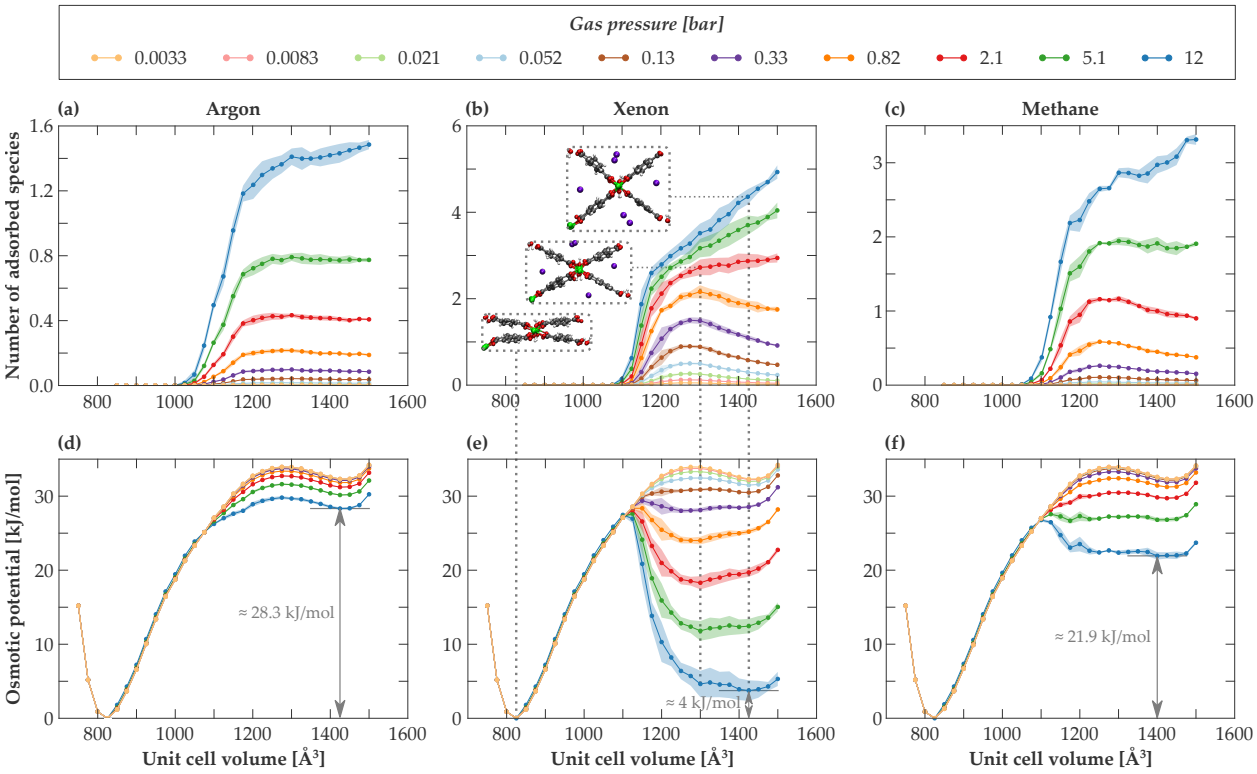

Figure 4: **(a–c)** Rigid-host adsorption isotherms for **(a)** argon, **(b)** xenon, and **(c)** methane as a function of the MIL-53(Al) unit cell volume V at 300 K for a range of pressures between 3.3×10^{-3} bar and 12 bar. **(d–f)** Corresponding osmotic potentials Ω as a function of the unit cell volume V for these three guest species. Shaded areas denote the 1σ uncertainty interval as determined over five independent simulations.

in MIL-53(Al), as illustrated in Figure S4 in the Supporting Information. As a result of this low uptake, the coresponding osmotic potentials, shown in Figure 4(d), exhibit two minima. These minima correspond with a stable, guest-free closed-pore (cp) phase at small volumes, which does not change with increasing gas pressure as no guests are adsorbed, and a metastable lp phase that is significantly less stable. Since the adsorption of neon nor argon is able to significantly affect the relative stability of the empty-host (meta)stable states of MIL-53(Al), Scheme 1 predicts that these guest species do not have the potential to induce structural transitions in MIL-53(Al) at room temperature.

For xenon, in contrast, Scheme 1 predicts an appreciable gas uptake. Depending on the gas pressure or, equivalently, the chemical potential, two types of xenon isotherms may be distinguished in Figure 4(b). For low to intermediate pressures, the uptake reaches a

maximum for intermediate states with a cell volume around 1250–1300 Å^3. At this volume, the diameter of the MIL-53(Al) 1D channel amounts to about 5 Å (see Figure S3 of the Supporting Information), which is slightly larger than the kinetic diameter of xenon. This ensures that each xenon atom can interact favorably with the organic linkers delimiting the 1D channel, thereby minimizing the adsorption energy (see insets in Figure 4(b) and Figure S4 in the Supporting Information). Consequently, xenon adsorption leads to the stabilization of a xenon-filled narrow-pore (np) phase, inducing a local minimum in the osmotic potentials of Figure 4(e) at this volume. At a gas pressure of 5.1 bar, for instance, xenon induces a np metastable minimum at a volume of about 1300 Å^3.

When further increasing the gas pressure, additional xenon atoms are forced inside the framework. As the xenon uptake at these highest pressures can only be increased further by increasing the unit cell volume, the adsorption isotherms at these high gas pressures no longer show a local maximum, but rather continue to increase with increasing cell volume. This is also revealed in the osmotic potentials, in which the np metastable minimum disappears in favor of the lp metastable minimum at ca. 1425 Å^3, which is only about 4 kJ/mol less stable than the cp phase at a gas pressure of 12 bar. The xenon-filled np and lp phases can both be stabilized further by decreasing the temperature, as discussed in Figure S2 of the Supporting Information, and the lp phase becomes the most stable phase at a gas pressure of 12 bar for temperatures below 250 K. Scheme 1 therefore correctly predicts that xenon may induce a phase transition in MIL-53(Al), in qualitative agreement with experiment.[50] However, the inaccuracy associated with Scheme 1 prohibits a quantitative prediction of the adsorption-induced lp volume. For instance, at a xenon gas pressure of 12 bar, all volumes in between 1300 Å^3 and 1475 Å^3 lie within the 1σ uncertainty interval of the lp state.

3.1.2 Methane and Carbon Dioxide Adsorption

Experimentally, methane adsorption only induces phase transitions in MIL-53(Al) for temperatures lower than about 250 K, whereas carbon dioxide has been shown to induce phase

transitions for temperatures up to 350 K.[51,52] When constructing the methane rigid-host isotherms, shown in Figure 4(c), one indeed observes a behavior in between that of argon and xenon. While an intermediate maximum in the methane rigid-host isotherms is found for low to intermediate gas pressures, similar to xenon adsorption, the total uptake is only halve of that of xenon at the same gas pressure. As a result, the corresponding osmotic potentials of Figure 4(f) show an np or lp metastable minimum that is about 22 kJ/mol less stable than the cp global minimum, so that one expects the cp phase to be retained during methane adsorption at 300 K. However, also here the 1σ uncertainty intervals limit the accuracy with which this np or lp volume can be determined.

For carbon dioxide, the rigid-host isotherms and corresponding osmotic potentials, depicted in panes (a) and (d) of Figure 5, respectively, are similar to those observed for xenon. The intermediate np metastable minimum for carbon dioxide adsorption occurs at a volume of about 1100–1200 Å^3, which is lower than the volume of the np phase induced by xenon adsorption (Figure 4(e)). This is in line with the smaller kinetic diameter of carbon dioxide with respect to xenon as well as the minimum in adsorption energy appearing at a lower volume than for xenon in Figure S4 of the Supporting Information. For the highest gas pressures, the lp phase is again only 5 kJ/mol less stable than the cp phase, so that one expects that both phases may be encountered during carbon dioxide adsorption in MIL-53(Al) at room temperature, in qualitative correspondence with experimental literature.[51,52]

However, when contrasting the carbon dioxide rigid-host isotherms and osmotic potentials to those obtained for the other adsorbates, an even larger variability and therefore inaccuracy is apparent for the former as indicated by the larger 1σ uncertainty intervals. To investigate the origin of this larger variability, panes (b) and (c) of Figure 5 depict the rigid-host isotherms obtained by considering only one cell shape per unit cell volume instead of averaging over five cell shapes as for pane (a). Comparing panes (b) and (c), one observes that the two different cell shapes give rise to adsorption capacities that differ significantly for some unit cell volumes. At a volume of 1225 Å^3 (shaded in grey) and at a pressure

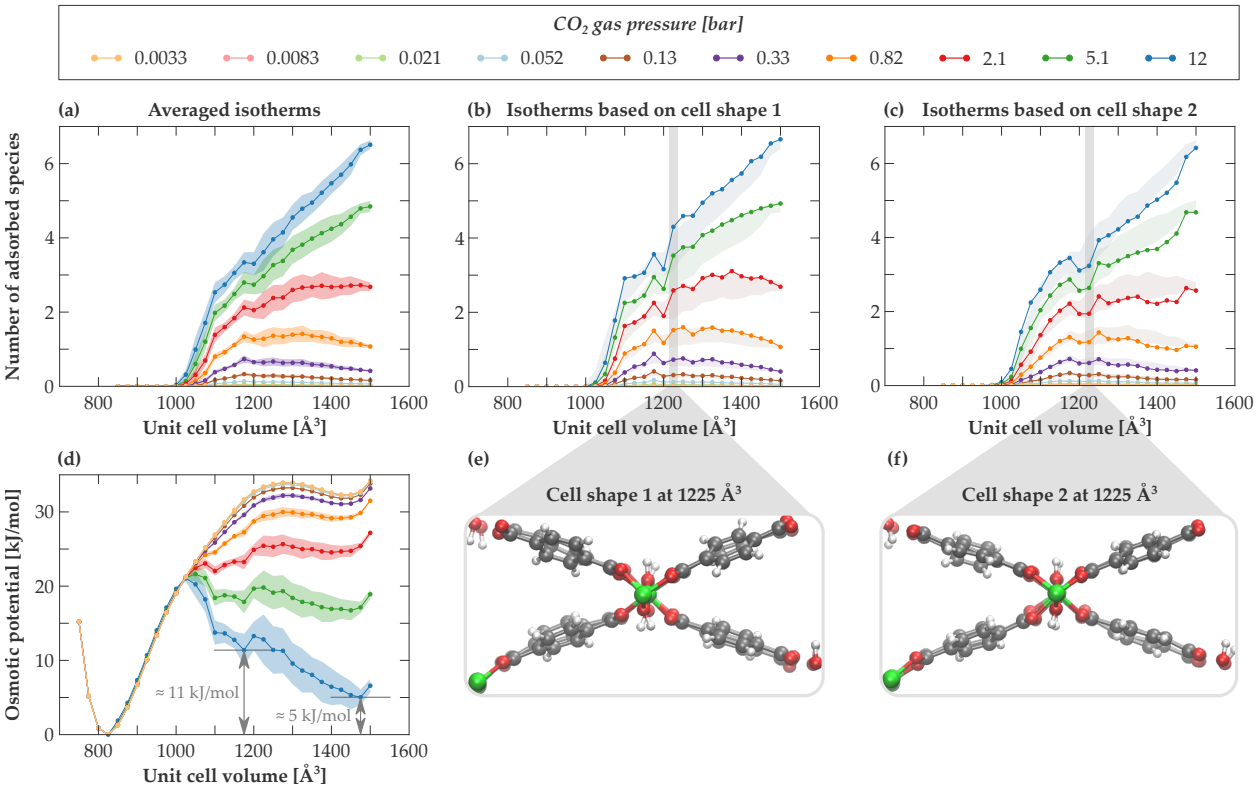

Figure 5: **(a–c)** Rigid-host adsorption isotherms for carbon dioxide as a function of the MIL-53(Al) unit cell volume V at 300 K for a range of pressures between 3.3×10^{-3} bar and 12 bar, obtained by **(b,c)** considering two different fixed cell shapes $\mathbf{h}_0$ and **(a)** averaged over GCMC simulations starting from five different cell shapes. **(d)** Corresponding osmotic potential Ω as a function of the unit cell volume V for the averaged isotherms. **(e–f)** The two MIL-53(Al) cell structures at 1225 Å^3 that give rise to the adsorption capacity shown in grey in panes (b) and (c). Shaded areas in panes (a) and (d) denote the 1σ uncertainty interval as determined over five independent simulations, and are repeated in panes (b) and (c) as a guide for the eye.

of 12 bar, for instance, the two simulations predict an average uptake of respectively 4.3 and 3.2 carbon dioxide molecules per unit cell, a difference of about 25%. Note that this difference does not arise from imprecision, as Section S1.4 of the Supporting Information indicates that the results are well converged. Rather, the observed discrepancy is only associated with insufficient sampling of the adsorption-induced flexibility of the framework in the $(N_{\text{host}}, \mu, V, \mathbf{h}_0, T)$ ensemble of Scheme 1. Indeed, visualizing the two MIL-53(Al) structures at 1225 Å^3 in panes (e) and (f) of Figure 5 shows a seemingly slight rotation of the phenyl moieties in the top right corner, which allows for a substantially more favorable interac-

tion with the adsorbed carbon dioxide molecules for cell shape 1 and therefore an increased gas uptake. This observation confirms that the rigid-host simulations of Scheme 1 are too crude to accurately sample adsorption in flexible MOFs, as it is in general impossible to quantitatively determine the volume of the adsorption-induced (meta)stable phases.

3.2 Scheme 2: Hybrid MC/MD Simulations in the Osmotic Ensemble

3.2.1 Noble Gas Adsorption

Figure 6 displays the results of Scheme 2 for xenon adsorption at three different temperatures. At 292 K, one observes two steps in the isotherm of Figure 6(a). For the lowest pressures, up to about 0.03 bar, the xenon uptake is negligible. Correspondingly, the predicted (meta)stable states in Figure 6(d) are the (empty) cp and lp states. For these lowest gas pressures, the phase observed during the simulation depends on the initialization: simulations initialized in the lp or cp state remain in the lp or cp state, respectively, as illustrated by the ten independent simulations shown in Figure 6. While, in theory, phase transitions between the lp and cp phases can be observed in this scheme, these phase transitions are rare events that are unlikely to occur during the simulation as both phases are separated by a high free energy barrier.

When increasing the gas pressure above 0.03 bar at 292 K, a first step in the adsorption isotherm is apparent, as xenon starts to adsorb in the material at this pressure. These adsorbates steer the framework from the cp or lp phase to the np phase with a volume of about 1250–1300 $Å^3$, as indicated in Figure 6(d). This observation is in excellent agreement with the xenon-loaded np volume extracted from Scheme 1 (Figure 4(e)). When further increasing the gas pressure, the uptake increases continuously to about four xenon atoms per unit cell, until reaching a pressure of 1 to 2 bar. At this pressure, a second step in the isotherm is observed, corresponding to a phase transition from the xenon-loaded np phase to

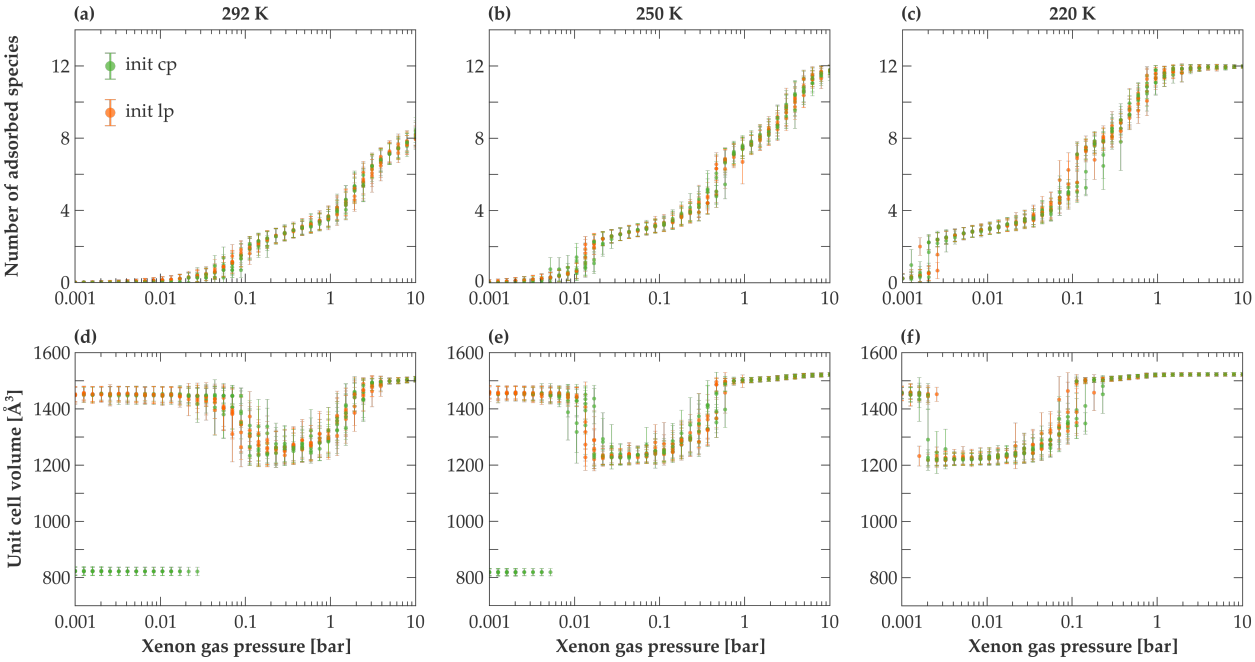

Figure 6: **(a–c)** Predicted number of adsorbed xenon atoms N_{Xe} and **(d–f)** MIL-53(Al) unit cell volumes V as a function of the xenon gas pressure p for three different temperatures: **(a,d)** $T = 292$ K, **(b,e)** $T = 250$ K, and **(c,f)** $T = 220$ K. At each temperature and gas pressure, ten simulations were performed: five starting in the cp state (green) and five starting in the lp state (orange). Error bars indicate the 1σ standard deviations of each separate simulation.

the xenon-loaded lp phase. At the maximum pressure of 10 bar considered here, a maximum loading of eight xenon atoms per unit cell is reached at 292 K.

When decreasing the temperature in Figure 6 to 250 K (panes (b) and (e)) and 220 K (panes (c) and (f)), the predicted isotherms and unit cell volumes as a function of the gas pressure retain their 292 K shapes. Decreasing the temperature only results in a decrease in the critical pressures necessary for the cp-to-np and the np-to-lp transitions, confirming the observations in Figure S2 of the Supporting Information that decreasing the temperature facilitates xenon-induced transitions in MIL-53(Al).

For neon and argon, no phase transitions are observed, as shown in Figures S7 and S8 of the Supporting Information, confirming the results of Scheme 1. For both adsorbates and at both temperatures, the MIL-53(Al) unit cell remains in the initial cp or lp state, irrespective of the gas pressure, confirming that transitions between both phases are activated processes.

3.2.2 Methane and Carbon Dioxide Adsorption

Figure 7(a) reveals a continuous methane adsorption isotherm at 292 K. The corresponding cell volumes in Figure 7(d) indeed show that MIL-53(Al) retains its original phase upon adsorption, with no intermediate np phase, in qualitative agreement with literature.[51,52] However, at methane pressures between 0.2 and 2 bar, one observes that the simulations initialized in the lp phase already start to explore smaller volumes during the simulation, with the lower limit of the 1σ uncertainty interval extending to about 1325 Å^3. By lowering the temperature to 230 K, the same stepwise behavior as encountered with xenon adsorption is observed. At this temperature, methane induces an lp-to-np transition at a pressure of ca. 0.2 bar, while an np-to-lp transition is induced at a pressure of ca. 1 bar. However, while Scheme 1 indicated that the methane-induced np phase would occur near a volume of about 1200 Å^3, the unit cell volumes at intermediate methane gas pressures vary here between 1200 Å^3 and 1500 Å^3. Visualizing the unit cell volume throughout the hybrid MC/MD procedure at such an intermediate gas pressure reveals spontaneous phase transitions between the np phase, at a volume of about 1200 Å^3, and the lp phase, at a volume of about 1475 Å^3 (see Figure S10 of the Supporting Information). These spontaneous phase transitions indicate that both the np and lp phases are (meta)stable states at this gas pressure, with a very small free energy barrier separating them, resulting in a large variation in the sampled unit cell volume during such a simulation. This impedes an accurate determination of the volumes associated with these (meta)stable states.

At 213 K, the stepwise behavior of the methane isotherm is even more pronounced. Both critical pressures necessary to induce a phase transition decrease with respect to their 230 K values. At this lower temperature, the frequency of the np-to-lp and lp-to-np phase transitions during a single simulation as observed at intermediate gas pressures also decreases due to an increased free energy barrier between both states and a lower thermal energy of the atoms. Furthermore, neither at 230 K nor at 213 K a cp-to-np transition is observed at these intermediate gas pressures, despite the metastability of the np phase. This is a direct

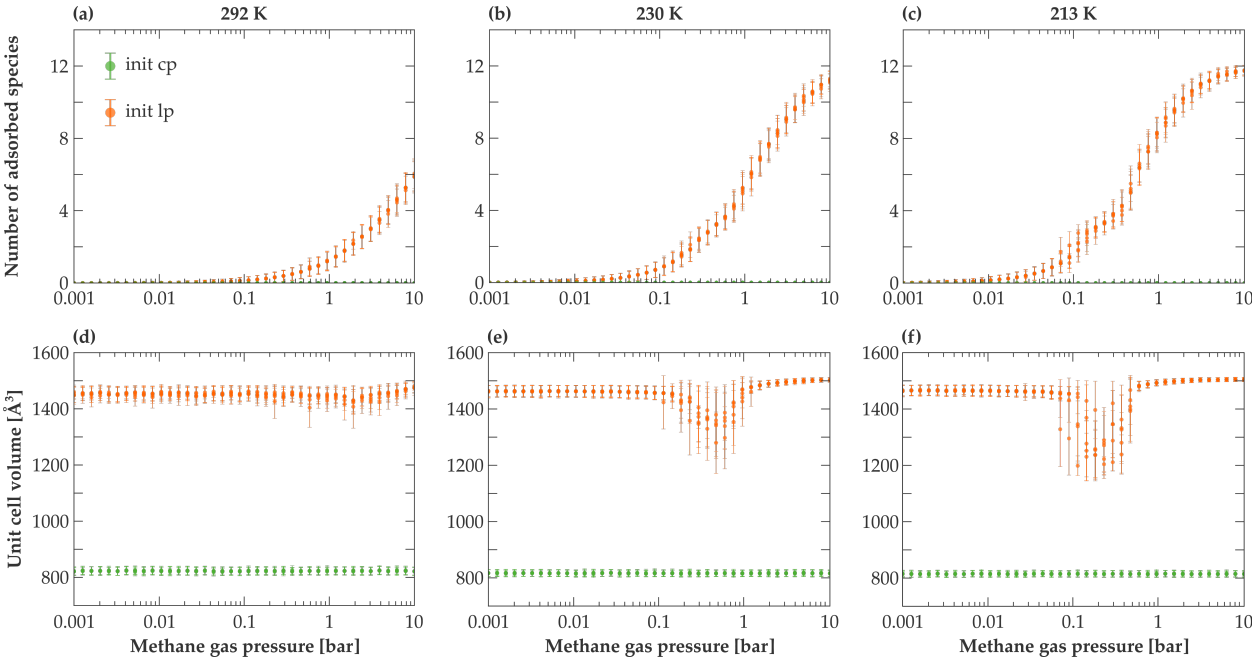

Figure 7: **(a–c)** Predicted number of adsorbed methane molecules N_{CH_4} and **(d–f)** MIL-53(Al) unit cell volumes V as a function of the methane gas pressure p for three different temperatures: **(a,d)** $T = 292$ K, **(b,e)** $T = 230$ K, and **(c,f)** $T = 213$ K. At each temperature and gas pressure, ten simulations were performed: five starting in the cp state (green) and five starting in the lp state (orange). Error bars indicate the 1σ standard deviations of each separate simulation.

consequence of the large energy barrier between both states, preventing these transitions from occurring spontaneously during the simulation.

For carbon dioxide, visualized in Figure S9 of the Supporting Information, two-step isotherms akin to the ones observed for xenon are obtained, in agreement with Scheme 1. Also here, decreasing the temperature results in a decrease in the critical gas pressures necessary to induce these phase transitions, in qualitative correspondence with experimental observations.[51]

In conclusion, the hybrid MC/MD protocol of Scheme 2 yields direct access to the adsorption isotherms and (meta)stable MIL-53(Al) states at a given gas pressure, in qualitative agreement with experiment.[51] However, a quantitative interpretation of these results is impeded due to two phenomena. First, premature phase transitions may occur if both phases are separated by very low barriers, such as for the lp-to-np transition under methane adsorp-

tion, making it impossible to exactly pinpoint the critical gas pressure necessary to induce this transition. Second, the phase space associated with the unit cell volume may not be sampled adequately if the (meta)stable states are separated by large free energy barriers, such as for the cp-to-np transition under methane adsorption. In that case, the initial state of the simulation affects the simulation results, such that multiple independent simulations need to be performed, reducing the efficiency of the procedure.

3.3 Scheme 3: Advanced MD Simulations of the Guest-Loaded Framework at Constant Volume

Figure 8(a–b) displays the pressure-versus-volume equations of state and corresponding free energy profiles for various xenon loadings in MIL-53(Al) at 300 K, obtained by application of Scheme 3. These profiles reveal the unit cell volumes of the (meta)stable states, which are plotted as a function of the xenon loading in Figure 8(c). The empty framework exhibits the well-known free energy profile with a stable cp phase at ca. 820 $Å^3$ and a metastable lp phase at ca. 1450 $Å^3$.[37,38] Upon forcing xenon into the framework, the global cp minimum vanishes immediately, while an intermediate np phase at a volume of about 1100 $Å^3$ is formed next to a very shallow lp phase. This lp phase disappears completely upon further increasing the xenon loading, while the stable np phase shifts to larger unit cell volumes reaching up to 1400 $Å^3$. Finally, when a loading of five xenon atoms per unit cell is reached, the lp state re-emerges in co-existence with the np state.

At first instance, these observations may seem to contradict the results of Schemes 1 and 2. First, both previous schemes predicted a stable cp phase also for low but nonzero xenon gas pressures, while here the cp minimum is only encountered for a zero xenon loading. However, this is a direct consequence of the guest loading being the control variable in this scheme rather than the gas pressure in Schemes 1 and 2, with a nontrivial relationship between both variables. Indeed, the xenon isotherms of Scheme 1 (Figure 4(b,e)) and Scheme 2 (Figure 6) predict that no xenon is adsorbed in the stable cp phase at low xenon gas pressures.

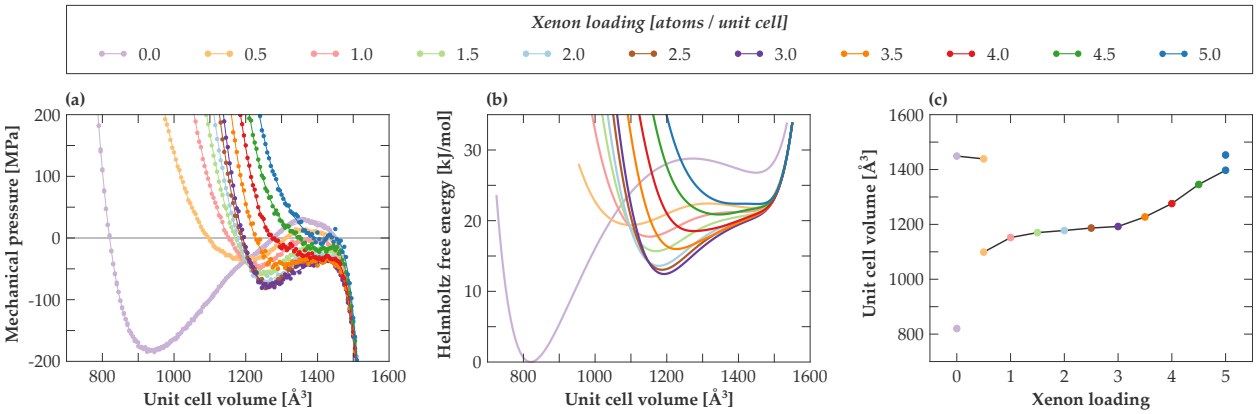

Figure 8: **(a)** Predicted pressure-versus-volume equation of state of MIL–53(Al) with various fixed xenon loadings at 300 K. **(b)** Corresponding Helmholtz free energy profiles at 300 K, and **(c)** unit cell volumes of the (meta)stable state(s) with increasing xenon loading. Figure reproduced from Ref. 19 with permission from Springer Nature.

Moreover, Figure 6 clearly reveals that a cp-to-np phase transition is triggered as soon as the cp initialized simulations start to adsorb xenon, confirming the observation of Scheme 3 that a stable cp phase cannot exist for a nonzero xenon loading. Second, the procedure outlined here predicts an np volume which starts to increase appreciably for xenon loadings between 3.5 and 5 atoms per unit cell, whereas the xenon-loaded np volume was found to be largely independent of the gas pressure in Figures 4 and 6. Once again, this results from fixing the xenon loading rather than the gas pressure or chemical potential. Figure 6(a) reveals that a xenon loading between 3.5 and 5 atoms per unit cell near 300 K corresponds to a very narrow range of gas pressures, between 1.0 and 1.5 bar, coinciding with the pressure necessary to induce an np-to-lp phase transition at this temperature. As a result, Figure 8(c) disproportionally highlights the volume dependence of the np phase.

In conclusion, while Scheme 3 succeeds in identifying all (meta)stable states independent of the free energy barriers between them, it only provides direct insight in the evolution of these (meta)stable states as a a function of the guest loading rather than the experimentally controlled gas pressure or chemical potential. To access the osmotic potential, one would need to further correlate the chemical potential with the number of adsorbed species at each unit cell volume, as outlined in Ref. 55. Furthermore, given the discrete and constant

number of guest species present in the unit cell, one has to rely on more expensive supercell simulations to predict the different (meta)stable states at fractional loadings, such as the $1 \times 2 \times 1$ supercell employed here to access half-integer loadings per unit cell.

3.4 Scheme 4: Hybrid MC/MD Simulations with a Flexible Unit Cell in the Restricted Osmotic Ensemble

Based on the results obtained so far, it is clear that none of the previous three schemes provides an ideal procedure to study gas adsorption in flexible MOFs. The rigid-host GCMC simulations of Scheme 1 are too crude to accurately predict adsorption isotherms and osmotic potentials, while the occurrence of premature phase transitions and high free energy barriers, which may not be surmounted in regular MD simulations, hinder the efficient application of Scheme 2. Finally, in Scheme 3, only the gas loading instead of the experimentally accessible chemical potential or gas pressure could be controlled, preventing a direct comparison with experiment. For this reason, we developed and validated a fourth scheme that alleviates these issues by explicitly accounting for the shape flexibility of the material. Compared to Scheme 1, the procedure of Scheme 4 can be expected to be more accurate and efficient. First off, by allowing fluctuations in the framework atoms in Scheme 4, the inaccuracy due to the artificial dependence on the initial atomic positions and cell shape that was present in Scheme 1 should be eliminated. Second, given that Scheme 4 is a completely hybrid MC/MD procedure, the MIL-53(Al) framework can adapt to accommodate for the different guest species during the simulation. In Scheme 1, this is inherently impossible, as one has to rely on one fixed framework per volume.

3.4.1 Noble Gas Adsorption

To investigate the performance of the newly proposed scheme, Scheme 4 is adopted to predict the adsorption isotherms and corresponding osmotic potentials for each of the five guest species in MIL-53(Al) at 300 K. In Figure 9, only the gases with the potential to induce phase

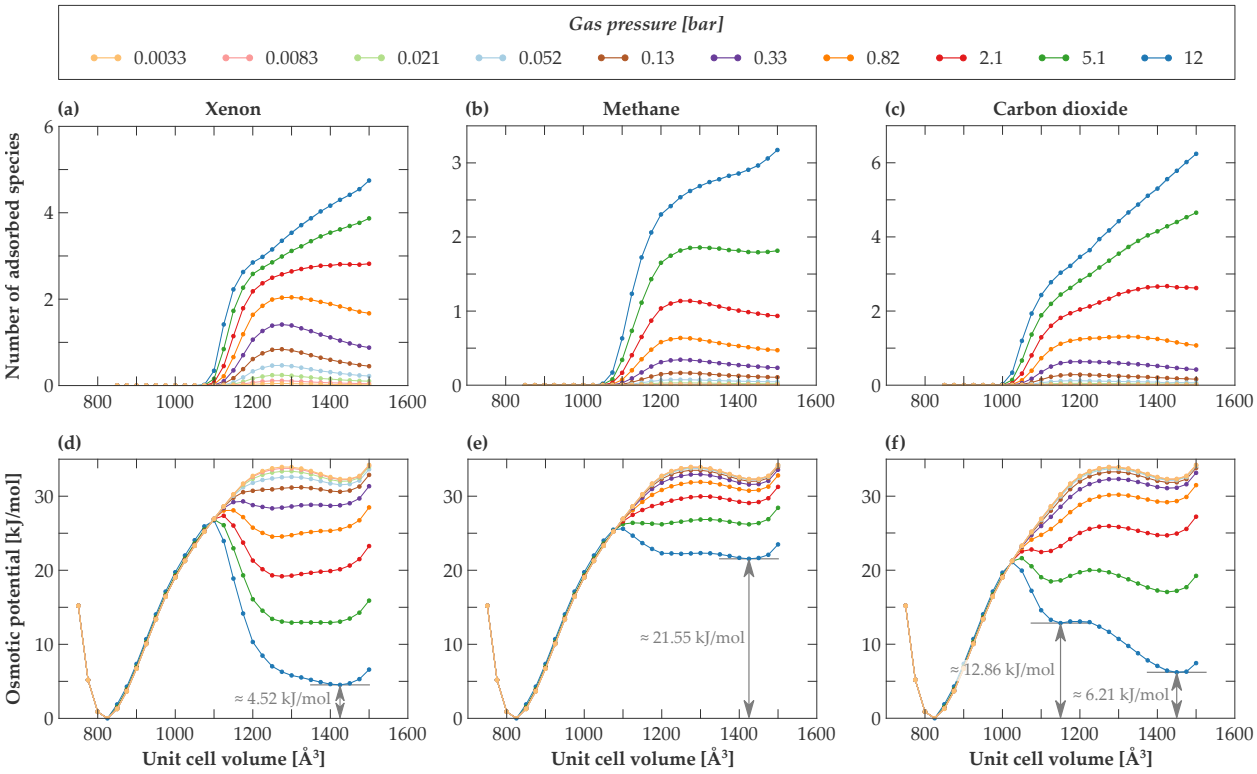

Figure 9: **(a–c)** Flexible-host adsorption isotherms for **(a)** xenon, **(b)** methane, and **(c)** carbon dioxide as a function of the MIL-53(Al) unit cell volume V at 300 K for a range of pressures between 3.3×10^{-3} bar and 12 bar as predicted from the newly introduced hybrid MC/MD scheme. **(d–f)** Corresponding osmotic potentials Ω as a function of the unit cell volume V for these three guest molecules. Shaded areas denote the 1σ uncertainty interval as determined over five independent simulations, which are negligible here.

transitions in MIL-53(Al)—xenon, methane, and carbon dioxide–are considered, whereas the results for neon and argon are displayed in Figure S14 of the Supporting Information.

Comparing the xenon flexible-host isotherm of Figure 9(a) with the corresponding rigid-host isotherm of Figure 4(b) immediately reveals that, while both types of isotherms share the same shape, an appreciably lower uncertainty is associated with the flexible-host isotherms of Scheme 4. Similar to the rigid-host isotherms, five independent flexible-host isotherms were constructed starting from five different cell shapes for each unit cell volume. In contrast to Scheme 1, however, our newly introduced scheme yields five sets of results which are virtually indistinguishable, as indicated by the very small 1σ uncertainty interval in Figure 9(d). For the metastable lp phase, this uncertainty is reduced almost hundredfold. This

confirms that the new procedure outlined here succeeds in fully accounting for the flexibility in the atomic positions and cell shape, so that the choice of initial snapshot does no longer artificially influence the obtained results. As a result, Scheme 4 requires only one hybrid MC/MD simulation per unit cell volume to obtain accurate results, improving the efficiency of the method.

This substantially improved accuracy does not only reduce the number of independent simulations that need to be carried out to get significant results, but also allows to quantitatively predict the evolution of the adsorption isotherm and (meta)stable states with increasing gas pressure. As an example, while it was impossible to extract from Figure 4(e) the exact metastable lp volume at a xenon gas pressure of 12 bar—only a broad volume range between 1300 Å^3 and 1475 Å^3 could be obtained—the osmotic potential of Figure 9(d) clearly indicates that the lp volume is found around 1425 Å^3. Moreover, Figure 4(e) hinted towards a possible metastable np phase at a pressure of 12 bar, with a volume around 1300 Å^3. However, when properly accounting for the flexibility in the host material, it becomes clear from Figure 9(d) that this np minimum only results from the large inaccuracy of Scheme 1.

3.4.2 Methane and Carbon Dioxide Adsorption

For methane adsorption at 300 K, the staggered osmotic potential of Figure 4(f) revealed multiple minima between 1100 Å^3 and 1400 Å^3 at the highest gas pressure, with an energy that fell within the 1σ uncertainty interval of the metastable lp minimum. In contrast, thanks to the increased accuracy of Scheme 4, Figure 9(e) demonstrates that only the lp state at a volume of 1425 Å^3 is a metastable state at 12 bar.

Undoubtedly, the increased accuracy of Scheme 4 is most pronounced for carbon dioxide. The rigid-host isotherms and osmotic potentials displayed in Figure 5 revealed a large dependence on the choice of the fixed framework during the GCMC procedure. As a result, it is difficult to uniquely determine from Figure 5(d) for which range of pressures an np phase

is induced, as well as to determine the relative stability of the various metastable phases. As a substantially lower uncertainty is associated with the flexible-host isotherms and osmotic potentials obtained in Scheme 4, which are displayed in Figure 9(c,f), these questions can now be fully answered. Figure 9(f) reveals that an np phase starts to appear at a carbon dioxide pressure of ca. 2.1 bar, while it almost disappears when increasing the pressure to 12 bar. With increasing pressure, the relative stability of the np and lp phases with respect to the cp phase increases, yielding metastable lp and np state at 12 bar which are about 6.21 kJ/mol and 12.86 kJ/mol less stable than the stable cp state at 12 bar.

In conclusion, these observations confirm the improved accuracy of the flexible-host isotherms, obtained by explicitly accounting for the flexibility of the host material in Scheme 4. This allows to quantitatively predict the number of adsorbed guest species as well as the different metastable states of the adsorbent at a given gas pressure. Furthermore, Scheme 4 prevents the need for multiple independent runs to improve the accuracy of the prediction, as one hybrid MC/MD simulation per unit cell volume is sufficient to obtain accurate results in good agreement with experiment. As a result, adoption of this scheme, which is freely available in the in-house `Yaff` software code,[56] to model gas adsorption in flexible adsorbents has to potential to further speed up the computer-aided discovery of interesting nanoporous materials for adsorption applications.

4 Conclusions

To adopt flexible MOFs for applications in gas storage, it is crucial to understand at a microscopic level how the interactions between the adsorbate and the adsorbent can be tuned in order to design the optimal MOF for a given application. In this respect, the insights provided by computational research could be unparallelled, given the existence of a computational procedure that can efficiently and accurately predict the adsorption isotherms and adsorption-induced flexibility in MOFs. While multiple schemes have been proposed for

this purpose, the extreme flexibility present in some MOFs may limit the applicability and accuracy of the results obtained with these schemes.

Therefore, the performances of four hybrid MC/MD simulation protocols to predict the adsorption of neon, argon, xenon, methane, and carbon dioxide in MIL-53(Al) were critically compared, focussing on their accuracy and efficiency. In a first scheme, rigid-host isotherms and associated osmotic potentials as a function of the unit cell volume were constructed. While this procedure is fast and solely relies on a set of GCMC simulations, it does not properly account for the flexibility in the atomic positions and cell shape of the host structure. As a consequence, the results obtained with this scheme were found to depend on the choice of the fixed framework used as input for the GCMC procedure, yielding differences of up to 25% in predicted carbon dioxide uptake caused by a small rotation in the organic linkers of MIL-53(Al). In a second scheme, hybrid MC/MD simulations were performed to obtain the equilibrium loadings and unit cell volume at a given gas pressure. This scheme, which directly samples the osmotic ensemble, was hindered by both premature phase transitions—a consequence of very small free energy barriers and internal pressure fluctuations during the simulations—and suppressed phase transitions—a consequence of the metastable states being separated by too high an energy barrier. Finally, in the third scheme, the Helmholtz free energy and equilibrium volumes as a function of the guest loading were determined. The main disadvantage of this last scheme was the lack of direct information on the osmotic potential, as the procedure samples at constant guest loading rather than at the experimentally controlled constant chemical potential or gas pressure.

Given the absence of a satisfactory procedure to study gas adsorption in flexible MOFs, a new hybrid procedure that is specifically designed to account for the flexibility of the host material was derived. In this novel scheme, flexible-host isotherms were constructed via hybrid MC/MD simulations during which the atomic positions and cell shape were allowed to fluctuate, while still controlling the cell volume. Application of this procedure to each of the five guest species indicated that the accuracy obtained with this scheme substantially out-

performs that of the other three schemes, as the artificial dependence on the fixed framework of Scheme 1 is no longer present. As a result, only one set of hybrid MC/MD simulations was sufficient to accurately predict the potential of these guest molecules to induce phase transitions in MIL-53(Al), furthermore obtaining a strong agreement with experiment. Moreover, this increased accuracy also results in a quantitative prediction of the different adsorption-induced metastable states at a given gas pressure. Therefore, this new and efficient scheme has the potential to further accelerate the computer-aided discovery of flexible MOFs for adsorption applications.

5 Computational Details

The four simulation schemes discussed here were implemented and tested in Yaff, our freely available in-house developed software package,[56] and validated extensively using RASPA[57] (see Section S4 in the Supporting Information). The temperature was controlled using a single Nosé-Hoover chain consisting of three beads and with a relaxation time $\tau_T = 0.1$ ps, which was coupled to both the particles and the barostat if applicable.[58–61] If necessary, the pressure P and/or deviatoric stress $\boldsymbol{\sigma}_a$ were controlled using a Martyna-Tobias-Tuckerman-Klein (MTTK) barostat with a relaxation time of 1 ps.[62,63] This combination of relaxation times promotes a complete yet efficient sampling of the accessible phase space.[37] To efficiently evaluate the long-range van der Waals and electrostatic interactions, a smooth cutoff at 15 Å was introduced and supplemented with analytical tail corrections. Specifically, the electrostatic interactions were calculated using an Ewald summation with a splitting parameter α of 0.213 Å^{-1} and a reciprocal space cutoff of 0.32 Å^{-1}.[64] For the MD simulations, a time step of 0.5 fs was employed to ensure energy conservation.

MIL-53(Al) was modeled using a $1\times2\times1$ cell containing 152 atoms, obtained by doubling the unit cell along the inorganic chain, and employing a force field generated from periodic *ab initio* data following the QuickFF procedure.[65] For the non-covalent MIL-53(Al) force

field parameters, atomic charges were obtained according to the Minimal Basis Iterative Stockholder (MBIS) partitioning scheme[66] as implemented in HORTON.[67] The all-electron density necessary for the MBIS scheme was obtained via a GPAW calculation.[68–70] For the GCMC simulations in Schemes 1 and 4, the van der Waals interactions were described using the Lennard-Jones (LJ) 12–6 interatomic potentials that are strongly positive for small internuclear distances, which is important for the insertion trial moves.[71] These LJ parameters were obtained from the MM3 parameters found in literature by requiring that the location and depth of the potential well are the same in both descriptions. In accordance with our earlier work on Scheme 3,[19,37] the MM3 Buckingham potentials were adopted to describe the van der Waals interactions in Schemes 2 and 3.[72] To prevent the insertion of particles in the unphysical regions at very small internuclear distances in Scheme 2, the MM3 potential was modified to reach a plateau equal to the maximum in the non-modified MM3 potential. The MM3 parameters, σ and ε, for both the MIL-53(Al) framework atoms and the guest species were obtained from Ref. 72 and were modified to the LJ form if necessary. For methane, a neutral united-atom model was employed, following the description of Ref. 73. Furthermore, an atomic point charge model was adopted for carbon dioxide, with partial charges of $0.6512|e|$ and $-0.3256|e|$ for the carbon and oxygen atoms, respectively, which complement the atomic MM3 parameters.[74] In the MC simulations, the carbon dioxide molecules were assumed to be rigid, whereas a flexible model was employed in the MD simulations. For the latter, the covalent force field terms were obtained using the QuickFF procedure.[65] As shown in Section S5 of the Supporting Information, the predicted gas adsorption isotherms are robust with respect to small changes in the host-guest interactions.

In Scheme 1, the GCMC simulations in the $(N_{\text{host}}, \mu, V, \mathbf{h}_0, T)$ ensemble were performed for a range of framework volumes V between 850 Å^3 and 1500 Å^3 with a step size of 25 Å^3, and for a series of chemical potentials μ. The snapshots of the empty framework structures were extracted from prior MD simulations in the $(N_{\text{host}}, N_{\text{guest}} = 0, P, \boldsymbol{\sigma}_a = \mathbf{0}, T)$ ensemble, starting in the lp phase and performed at a sufficiently high pressure in order to initiate

an lp-to-cp transition. During these MC simulations, four types of MC moves were tried: insertion of the guest molecule in the framework, deletion of the guest molecule from the framework, translation of the guest molecule, and rotation of the guest molecule in the case of CO_2. As indicated in Section S1.3 of the Supporting Information, an equal probability of proposing these moves leads to an optimal convergence. A total number of 750 000 MC steps were performed for xenon, methane, and carbon dioxide, whereas this was decreased to 500 000 and 250 000 MC steps for argon and neon, respectively. As discussed in Section S1.4 of the Supporting Information, this simulation length ensures a full convergence of the obtained results. To shed light on the possible influence of the flexibility of the framework on the obtained results, five different structures—with differing cell shapes $\mathbf{h}_0$ and atomic positions but with the same volume—were considered at each volume point between 850 Å^3 and 1500 Å^3, and the results reported here were averaged over these five simulations with associated 1σ uncertainty intervals unless indicated otherwise.

In Scheme 2, the rate of convergence of the hybrid procedure was maximized by considering MD runs of 400 steps (0.2 ps) each and proposing this move with a probability of 1:400 compared to each of the other MC moves (insertion, deletion, translation, and, if necessary, rotation), as outlined in more detail in Sections S2.2 and S2.3 of the Supporting Information. To improve the probability of acceptance and hence accelerate the convergence of the method, acceptance and rejection windows rather than single acceptance and rejection snapshots are considered for the MD trajectories, as introduced in Ref. 75 and outlined in more detail in Section S2.4 of the Supporting Information. Here, the size of these windows was chosen to equal halve the total simulation length, so that each step in the MD simulation can be selected as the new state in the MC procedure. To determine the variability in the obtained results, ten independent simulations were performed for each chemical potential μ, or equivalently, gas pressure p. Five of these simulations started from the empty lp phase, while the other five started from the empty cp phase. A total number of 3 000 000 MC steps were performed for argon, xenon, and methane, while 2 000 000 and 5 000 000 MC steps were

performed for neon and carbon dioxide, respectively.

In Scheme 3, the $(N_{\text{host}}, N_{\text{guest}}, V, \boldsymbol{\sigma}_a = \mathbf{0}, T)$ simulations were performed for various guest loadings N_{guests} varying between 0 and 5 xenon atoms. As a $1 \times 2 \times 1$ supercell is used, it is also possible to probe at half integer guest loadings. For all simulations of Scheme 3, a production run of 700 ps was considered, which was preceded by a 100 ps equilibration run.

In Scheme 4, five structures with differing initial cell shapes $\mathbf{h}_0$ and atomic positions but with the same volume were considered at each volume point between 850 Å^3 and 1500 Å^3, and the results reported here were averaged over these five simulations, similar to Scheme 1. As in Scheme 2, a total number of 3 000 000 MC steps were performed for argon, xenon, and methane, while 2 000 000 and 5 000 000 MC steps were performed for neon and carbon dioxide, respectively.

Finally, to relate the chemical potential μ and the gas pressure p at a given temperature T, the free energy of a van der Waals gas is adopted:

$$\mu(p,T) = k_B T \ln \frac{b\rho}{1-b\rho} + k_B T \frac{b\rho}{1-b\rho} - 2a\rho + \mu_0 - k_B T \ln \frac{p_0 b}{k_B T}; \tag{5.1a}$$

$$p(\rho,T) = k_B T \frac{\rho}{1-b\rho} - a\rho^2. \tag{5.1b}$$

In this formula, k_B is the Boltzmann's constant and $\rho(p,T)$ is the number density of the gas, obtained from the van der Waals equation of state at the given pressure and temperature. The parameters μ_0 and p_0 are the reference chemical potential and pressure, and a and b describe the interactions between the guest molecules and the volume taken up by these guest molecules, respectively. The a and b parameters for the adsorbates discussed in this work are summarized in Table 1.

Table 1: The van der Waals parameters a and b entering Eq. (5.1) for the various adsorbates discussed in this work.[76]

guest species	$\boldsymbol{a}$ **[$\ell^2 \cdot$ bar / mol]**	$\boldsymbol{b}$ **[ℓ /mol]**
neon	0.214	0.01710
argon	1.355	0.03200
xenon	4.250	0.05105
methane	2.283	0.04280
carbon dioxide	3.640	0.04280

Author Information

Corresponding Author

*E-mail: Veronique.VanSpeybroeck@UGent.be

Notes

The authors declare no competing financial interest.

Acknowledgement

This research was funded by the Fund for Scientific Research—Flanders (FWO), the Research Board of Ghent University (BOF), and the European Union's Horizon 2020 research and innovation programme (consolidator ERC grant agreement number 647755–DYNPOR (2015–2020)). The computational resources and services used in this work were provided by the Flemish Supercomputer Center (VSC), funded by the Hercules foundation and the Flemish Government—department EWI. J.J. G.-S. acknowledges the Research Council of Ghent University for his BOF-postdoctoral fellowship.

Supporting Information Available

The results of the four schemes for those gas species not considered in the main manuscript. The adsorption energy for each of the guest species. The convergence of the GCMC and hybrid MC/MD procedures. The validation of the Yaff results with RASPA. Sensitivity of the predicted gas adsorption isotherms on the non-covalent force field parameters.

References

(1) Mason, J. A.; Veenstra, M.; Long, J. R. *Chem. Sci.* **2014**, *5*, 32–51.

(2) He, Y.; Zhou, W.; Qian, G.; Chen, B. *Chem. Soc. Rev.* **2014**, *43*, 5657–5678.

(3) Li, H.; Wang, K.; Sun, Y.; Lollar, C. T.; Li, J.; Zhou, H.-C. *Mater. Today* **2018**, *21*, 108–121.

(4) Murray, L. J.; Dincă, M.; Long, J. R. *Chem. Soc. Rev.* **2009**, *38*, 1294–1314.

(5) Suh, M. P.; Park, H. J.; Prasad, T. K.; Lim, D.-W. *Chem. Rev.* **2012**, *112*, 782–835.

(6) Liu, J.; Thallapally, P. K.; McGrail, B. P.; Brown, D. R.; Liu, J. *Chem. Soc. Rev.* **2012**, *5*, 2308–2322.

(7) Mondloch, J. E.; Katz, M. J.; Isley III, W. C.; Ghosh, P.; Liao, P.; Bury, W.; Wagner, G. W.; Hall, M. G.; DeCoste, J. B.; Peterson, G. W.; Snurr, R. Q.; Cramer, C. J.; Hupp, J. T.; Farha, O. K. *Nat. Mater.* **2015**, *14*, 512–516.

(8) Li, H.; Eddaoudi, M.; O'Keeffe, M.; Yaghi, O. M. *Nature* **1999**, *402*, 276–279.

(9) Férey, G. *Chem. Mater.* **2001**, *13*, 3084–3098.

(10) Kitagawa, S.; Kitaura, R.; Noro, S.-i. *Angew. Chem., Int. Ed.* **2004**, *43*, 2334–2375.

(11) Zhou, H.-C.; Long, J. R.; Yaghi, O. M. *Chem. Rev.* **2012**, *112*, 673–674.

(12) Furukawa, H.; Cordova, K. E.; O'Keeffe, M.; Yaghi, O. M. *Science* **2013**, *341*, 1230444.

(13) Maurin, G.; Serre, C.; Cooper, A.; Férey, G. *Chem. Soc. Rev.* **2017**, *46*, 3104–3107.

(14) Eddaoudi, M.; Kim, J.; Rosi, N.; Vodak, D.; Wachter, J.; O'Keeffe, M.; Yaghi, O. M. *Science* **2002**, *295*, 469–472.

(15) Yaghi, O. M.; O'Keeffe, M.; Ockwig, N. W.; Chae, H. K.; Eddaoudi, M.; Kim, J. *Nature* **2003**, *423*, 705–714.

(16) Li, J.-R.; Sculley, J.; Zhou, H.-C. *Chem. Rev.* **2012**, *112*, 869–932.

(17) Li, X.; Liu, Y.; Wang, J.; Gascon, J.; Li, J.; Van der Bruggen, B. *Chem. Soc. Rev.* **2017**, *46*, 7124–7144.

(18) Kang, Z.; Fan, L.; Sun, D. *J. Mater. Chem. A* **2017**, *5*, 10073–10091.

(19) Vanduyfhuys, L.; Rogge, S. M. J.; Wieme, J.; Vandenbrande, S.; Maurin, G.; Waroquier, M.; Van Speybroeck, V. *Nat. Commun.* **2018**, *9*, 204.

(20) Chowdhury, P.; Bikkina, C.; Meister, D.; Dreisbach, F.; Gumma, S. *Microporous Mesoporous Mater.* **2009**, *117*, 406–413.

(21) Coudert, F.-X.; Boutin, A.; Jeffroy, M.; Mellot-Draznieks, C.; Fuchs, A. H. *ChemPhysChem* **2011**, *12*, 247–258.

(22) Schneemann, A.; Bon, V.; Schwedler, I.; Senkovska, I.; Kaskel, S.; Fischer, R. A. *Chem. Soc. Rev.* **2014**, *43*, 6062–6096.

(23) Coudert, F.-X.; Fuchs, A. H. *Coord. Chem. Rev.* **2016**, *307*, 211–236.

(24) Vandenbrande, S.; Verstraelen, T.; Gutiérrez-Sevillano, J. J.; Waroquier, M.; Van Speybroeck, V. *J. Phys. Chem. C* **2017**, *121*, 25309–25322.

(25) Lin, L.-C.; Berger, A. H.; Martin, R. L.; Kim, J.; Swisher, J. A.; Jariwala, K.; Rycroft, C. H.; Bhown, A. S.; Deem, M. W.; Haranczyk, M.; Smit, B. *Nat. Mater.* **2012**, *11*, 633–641.

(26) Fischer, M.; Gomes, J. R. B.; Fröba, M.; Jorge, M. *Langmuir* **2012**, *28*, 8537–8549.

(27) Fang, H. J.; Demir, H.; Kamakoti, P.; Sholl, D. S. *J. Mater. Chem. A* **2014**, *2*, 274–291.

(28) Vandenbrande, S.; Waroquier, M.; Van Speybroeck, V.; Verstraelen, T. *J. Chem. Theory Comput.* **2018**, In revision.

(29) Férey, G.; Serre, C. *Chem. Soc. Rev.* **2009**, *38*, 1380–1399.

(30) Coudert, F.-X. *Chem. Mater.* **2015**, *27*, 1905–1916.

(31) Fairen-Jimenez, D.; Moggach, S. A.; Wharmby, M. T.; Wright, P. A.; Parsons, S.; Düren, T. *J. Am. Chem. Soc.* **2011**, *133*, 8900–8902.

(32) Mellot-Draznieks, C.; Serre, C.; Surblé, S.; Audebrand, N.; Férey, G. *J. Am. Chem. Soc.* **2005**, *127*, 16273–16278.

(33) Serre, C.; Mellot-Draznieks, C.; Surblé, S.; Audebrand, N.; Filinchuk, Y.; Férey, G. *Science* **2007**, *315*, 1828–1831.

(34) Loiseau, T.; Serre, C.; Huguenard, C.; Fink, G.; Taulelle, F.; Henry, M.; Bataille, T.; Férey, G. *Chem.—Eur. J.* **2004**, *10*, 1373–1382.

(35) Liu, Y.; Her, J.-H.; Dailly, A.; Ramirez-Cuesta, A. J.; Neumann, D. A.; Brown, C. M. *J. Am. Chem. Soc.* **2008**, *130*, 11813–11818.

(36) Beurroies, I.; Boulhout, M.; Llewellyn, P. L.; Kuchta, B.; Férey, G.; Serre, C.; Denoyel, R. *Angew. Chem., Int. Ed.* **2010**, *49*, 7526–7529.

(37) Rogge, S. M. J.; Vanduyfhuys, L.; Ghysels, A.; Waroquier, M.; Verstraelen, T.; Maurin, G.; Van Speybroeck, V. *J. Chem. Theory Comput.* **2015**, *11*, 5583–5597.

(38) Demuynck, R.; Rogge, S. M. J.; Vanduyfhuys, L.; Wieme, J.; Waroquier, M.; Van Speybroeck, V. *J. Chem. Theory Comput.* **2017**, *13*, 5861–5873.

(39) Rogge, S. M. J.; Waroquier, M.; Van Speybroeck, V. *Acc. Chem. Res.* **2018**, *51*, 138–148.

(40) Rogge, S. M. J.; Caroes, S.; Demuynck, R.; Waroquier, M.; Van Speybroeck, V.; Ghysels, A. *J. Chem. Theory Comput.* **2018**, *14*, 1186–1197.

(41) Evans, J. D.; Coudert, F.-X. *J. Phys. Chem. Lett.* **2017**, *8*, 1578–1584.

(42) Duane, S.; Kennedy, A. D.; Pendleton, B. J.; Roweth, D. *Phys. Lett. B* **1987**, *195*, 216–222.

(43) Mehlig, B.; Heermann, D. W.; Forrest, B. M. *Phys. Rev. B* **1992**, *45*, 679–685.

(44) Faller, R.; de Pablo, J. J. *J. Chem. Phys.* **2002**, *116*, 55–59.

(45) Jeffroy, M.; Fuchs, A. H.; Boutin, A. *Chem. Commun.* **2008**, 3275–3277.

(46) Coudert, F.-X.; Jeffroy, M.; Fuchs, A. H.; Boutin, A.; Mellot-Draznieks, C. *J. Am. Chem. Soc.* **2008**, *130*, 14294–14302.

(47) Greathouse, J. A.; Kiniburgh, T. L.; Allendorf, M. D. *Ind. Eng. Chem. Res.* **2009**, *48*, 3425–3431.

(48) Witman, M.; Ling, S.; Jawahery, S.; Boyd, P. G.; Haranzcyk, M.; Slater, B.; Smit, B. *J. Am. Chem. Soc.* **2017**, *139*, 5547–5557.

(49) Ghoufi, A.; Maurin, G. *J. Phys. Chem. C* **2010**, *114*, 6496–6502.

(50) Boutin, A.; Springuel-Huet, M.-A.; Nossov, A.; Gédéon, A.; Loiseau, T.; Volkringer, C.; Férey, G.; Coudert, F.-X.; Fuchs, A. H. *Angew. Chem., Int. Ed.* **2009**, *48*, 8314–8317.

(51) Boutin, A.; Coudert, F.-X.; Springuel-Huet, M.-A.; Neimark, A. V.; Férey, G.; Fuchs, A. H. *J. Phys. Chem. C* **2010**, *114*, 22237–22244.

(52) Bourrelly, S.; Llewellyn, P. L.; Serre, C.; Millange, F.; Loiseau, T.; Férey, G. *J. Am. Chem. Soc.* **2005**, *127*, 13519–13521.

(53) Mehta, M.; Kofke, D. A. *Chem. Eng. Sci.* **1994**, *49*, 2633–2645.

(54) Kirkwood, J. G. *J. Chem. Phys.* **1935**, *3*, 300–313.

(55) Vanduyfhuys, L.; Ghysels, A.; Rogge, S. M. J.; Demuynck, R.; Van Speybroeck, V. *Mol. Simulat.* **2015**, *41*, 1311–1328.

(56) Verstraelen, T.; Vanduyfhuys, L.; Vandenbrande, S.; Rogge, S. M. J. *Yaff, Yet Another Force Field*, Available online at http://molmod.ugent.be/software/.

(57) Dubbeldam, D.; Calero, S.; Ellis, D. E.; Snurr, R. Q. *Mol. Simul.* **2016**, *42*, 81–101.

(58) Nosé, S. *Mol. Phys.* **1984**, *52*, 255–268.

(59) Nosé, S. *J. Chem. Phys.* **1984**, *81*, 511–519.

(60) Hoover, W. G. *Phys. Rev. A* **1985**, *31*, 1695–1697.

(61) Martyna, G. J.; Klein, M. L.; Tuckerman, M. E. *J. Chem. Phys.* **1992**, *97*, 2635–2643.

(62) Martyna, G. J.; Tobias, D. J.; Klein, M. L. *J. Chem. Phys.* **1994**, *101*, 4177–4189.

(63) Martyna, G. J.; Tuckerman, M. E.; Tobias, D. J.; Klein, M. L. *Mol. Phys.* **1996**, *87*, 1117–1157.

(64) Ewald, P. P. *Ann. Phys.* **1921**, *369*, 253–287.

(65) Vanduyfhuys, L.; Vandenbrande, S.; Wieme, J.; Waroquier, M.; Verstraelen, T.; Van Speybroeck, V. *J. Comput. Chem.* **2018**, *39*, 999–1011.

(66) Verstraelen, T.; Vandenbrande, S.; Heidar-Zadeh, F.; Vanduyfhuys, L.; Van Speybroeck, V.; Waroquier, M.; Ayers, P. W. *J. Chem. Theory Comput.* **2016**, *12*, 3894–3912.

(67) Verstraelen, T.; Boguslawski, K.; Tecmer, P.; Heidar-Zadeh, F.; Chan, M.; Kim, T. D.; Zhao, T.; Vandenbrande, S.; Yang, D.; González-Espinoza, C. E.; Limacher, P. A.; Berrocal, D.; Malek, A.; Ayers, P. W. 2015; HORTON 2.0.0, http://theochem.github.com/horton/.

(68) Mortensen, J. J.; Hansen, L. B.; Jacobsen, K. W. *Phys. Rev. B* **2005**, *71*, 035109.

(69) Enkovaara, J.; Rostgaard, C.; Mortensen, J. J.; Chen, J.; Dułak, M.; Ferrighi, L.; Gavnholt, J.; Glinsvad, C.; Haikola, V.; Hansen, H. A.; Kristoffersen, H. H.; Kuisma, M.; Larsen, A. H.; Lehtovaara, L.; Ljungberg, M.; Lopez-Acevedo, O.; Moses, P. G.; Ojanen, J.; Olsen, T.; Petzold, V.; Romero, N. A.; Stausholm-Møller, J.; Strange, M.; Tritsaris, G. A.; Vanin, M.; Walter, M.; Hammer, B.; Häkkinen, H.; Madsen, G. K. H.; Nieminen, R. M.; Nørskov, J. K.; Puska, M.; Rantala, T. T.; Schiøtz, J.; Thygesen, K. S.; Jacobsen, K. W. *J. Phys. Condens. Matter* **2010**, *22*, 253202.

(70) Bahn, S. R.; Jacobsen, K. W. *Comput. Sci Eng.* **2002**, *4*, 56–66.

(71) Jones, J. E. *Proc. R. Soc. A* **1924**, *106*, 463–477.

(72) Lii, J. H.; Allinger, N. L. *J. Am. Chem. Soc.* **1989**, *111*, 8576–8582.

(73) Martin, M. G.; Siepmann, J. I. *J. Phys. Chem. B* **1998**, *102*, 2569–2577.

(74) Salles, F.; Ghoufi, A.; Maurin, G.; Bell, R. G.; Mellot-Draznieks, C.; Férey, G. *Angew. Chem., Int. Ed.* **2008**, *47*, 8487–8491.

(75) Neal, R. M. *J. Comput. Phys.* **1994**, *111*, 194–203.

(76) Rumble, J. R. *CRC Handbook of Chemistry and Physics*, 98th ed.; CRC Press, 2017.

TOC text

A hybrid simulation protocol to predict gas adsorption in flexible materials such as metal-organic frameworks is introduced and validated. This protocol relies on Monte Carlo and molecular dynamics steps that specifically sample the flexibility of the host material. The protocol is validated by investigating adsorption-induced breathing in MIL-53(Al) and results in a substantial increase in accuracy compared to current state-of-the-art protocols.

TOC keyword

Gas adsorption

Graphical TOC Entry